Journal of Applied Polymer Science

Hydrogen gas barrier property of polyelectrolyte/GO layer-by-layer films

Lili Zhao,[1] Haixiang Sun,[1] Namhoon Kim,[2] Joonghee Lee,[2] Ying Kong,[1] Peng Li[1]

[1]State Key Laboratory of Heavy Oil Processing, College of Chemical Engineering, China University of Petroleum, Huadong, Qingdao 266580, China

[2]Department of Polymer and Nano Engineering, BIN Fusion Research Team, Chonbuk National University, Jeonju, Jeonbuk, 561-756, South Korea

Correspondence to: P. Li (E-mail: lip@upc.edu.cn)

ABSTRACT: Different types of ultrathin multilayer composite membranes adsorbed on polyethylene terephthalate (PET) substrates are fabricated by the layer-by-layer (LBL) self-assembly technique. The hydrogen gas barrier performances of these membranes are measured using a pressure permeation instrument. Polyethylenimines/graphene oxide (PEI/GO) are chosen as the optimal system; the multilayer film reduces the hydrogen transmission rate of the uncoated PET film from 1357 to 24 $cm^3/(m^2$ 24 h 0.1 MPa). The membrane assembly process for the PEI/GO system is analyzed with UV–Visible spectroscopy, and the flat morphology of the ultrathin film is observed by scanning electron and atomic force microscopies. Moreover, in order to fully characterize the PEI/GO multilayer film system, we investigate the effects of multiple variables on the hydrogen resistance performance. These include the molecular weight of PEI, concentrations of PEI and GO, number of bilayers, soaking time, and drying methods. The film thickness is found to increase linearly during the LBL assembly process. © 2015 Wiley Periodicals, Inc. J. Appl. Polym. Sci. **2015**, *132*, 41973.

KEYWORDS: films; packaging; self-assembly

Received 5 August 2014; accepted 11 January 2015

DOI: 10.1002/app.41973

INTRODUCTION

Hydrogen, as an important industrial raw material, has many advantages as a fuel. For example, (1) hydrogen is a rich source of energy and can be obtained by the electrolysis of water. (2) Hydrogen has a high specific energy density, i.e., on a per kilogram basis, hydrogen can release more than three times the gasoline calorific value. (3) Hydrogen is one of the cleanest fuels because the product of its combustion is water. However, current challenges surrounding hydrogen storage and transportation limit its practical applications. Because of its low density and the relatively small size of its basic molecule, hydrogen requires a low liquefaction temperature and high pressure for large-volume transport. However, large compression pressures are not a practical option in this process, as small hydrogen molecules can easily escape through the storage cylinder. Additionally, the colorless, tasteless, and flammable hydrogen gas can diffuse quickly, which may lead to an explosion risk. Therefore, in order to reduce costs and ensure safety, good hydrogen barrier materials to be attached to the inner walls of hydrogen containers, need to be developed. High-barrier films have been shown to effectively prevent the infiltration of small-molecule gases.[1,2] Currently, oxide coatings (AlOx,[3] SiOx[4,5]), liquid-crystal polymers (LCPs),[6] and nanoplatelets (clay[7] and layered silicate[8]) are used to prepare composite films with polymers. These composite films combine the good mechanical properties of the polymer with the excellent barrier performance of the inorganic thin film. As a result, there has been a great deal of recent interest and research in high-barrier materials for gases.[7,8]

Layer-by-layer (LBL) assembly is a versatile method for the fabrication of multilayer films.[9,10] Different interaction forces are exploited in the LBL assembly technique, including the electrostatic force,[11] the hydrophobic force,[12] hydrogen bonding,[13] and covalent bonding.[14] To obtain a LBL deposited multilayer film, the selected substrate is alternately dipped into solutions of inorganic materials and oppositely charged polymers. Because of its simple operation, flexible method, and precise control, the LBL assembly technique has been widely used, and prepared multifunctional thin films have potential applications in permselective and gas-barrier membranes.[15,16]

Graphene, a relatively new material with a two-dimensional nanostructure, has attracted much attention in diverse scientific fields since its discovery in 2004.[17] Graphene comprises a single layer of sp^2-bonded carbon atoms with a high surface-to-

volume ratio, which provides it with unique electrical,[18,19] thermal,[20] and mechanical properties.[21] These unique properties have led to its moniker as "the material of the future," and graphene stands to play a significant role in the development of nanocomposites, electronic devices, and ultrathin membranes. Currently, many techniques are used to produce high quality graphene, such as micromechanical exfoliation,[17] epitaxial growth,[22] chemical vapor deposition,[23,24] and the reduction of graphene oxide (GO).[25] However, owing to the strong van der Waals attraction between the graphene layers, these methods fail to obtain stable single-layer sheets. This severely limits their use for fundamental studies and practical production.[26] To overcome this, graphene sheets have been functionalized with hydroxyl (OH) and epoxy groups on the basal plane and carboxylic acid (COOH) groups at the edges.[27] This GO is a single-atomic-layer sheet and prepared by the chemical oxidation and exfoliation of graphite. In contrast to graphene, GO can be stably dispersed in an aqueous solution without any stabilizing agent.[28] In water, the COOH groups on the edges of GO become negatively charged,[29] which causes the GO sheets to separate and adsorb on the cationic polyelectrolytes. Therefore, GO is a promising material for the preparation of nanocomposites. Furthermore, because of their high aspect ratio, the GO-based nanocomposites also exhibit better gas barrier properties,[30] similar to clay.

While there have been a few studies on the preparation of GO/polymer LBL films for gas barrier applications,[31–33] there remains a significant gap in the literature with respect to the level of experimental detail required to advance the field. This is particularly true for hydrogen gas barrier applications. However, most of the research is focus on oxygen and water vapor barrier. In this study, different types of positively charged polymers were chosen to prepare gas barrier films. The multilayer composite membranes adsorbed on a polyethylene terephthalate (PET) substrate were fabricated by the LBL self-assembly technique via electrostatic interactions. The assembly process and morphology of the membranes were analyzed, and the performances of the hydrogen gas barrier of the membranes were measured. Further, the best film with optimal gas barrier performance is identified. For the best system, detailed accounts are made of the effects of the drying method, dipping time, molecular weight of the polymer, number of bilayers, and feed concentration on the hydrogen resistance performance of the multilayer membranes.

EXPERIMENTAL

Materials

GO (oxidation degree >95%) in powder form was purchased from Chengdu Institute of Organic Chemistry, Academia Sinica, China. Single-layer GO (Figure 1) was exfoliated in ultrapure water by ultrasonication (200 W) for 30 min using a high-intensity sonicator (Sonics, Newtown, CT), and centrifuged for 30 min at 8000 rpm 20°C using a high-speed tabletop refrigerated centrifuge (Hanil Science Industrial Co., Ltd., Korea). The GO suspensions (0.1%, 0.5%, and 1%) were prepared by sonicating 200 mL solutions, and the GO suspensions were renewed every 10 depositions to prevent experimental error caused by

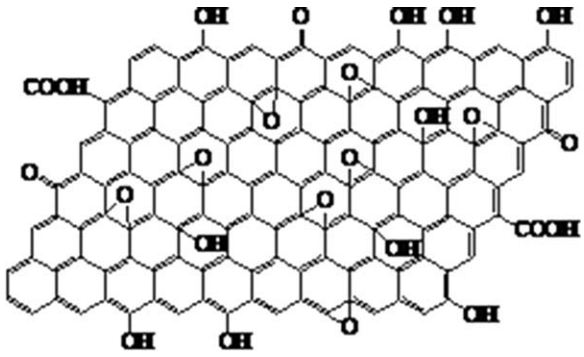

Figure 1. Single-layer GO sheet.

GO consumption. Pure polyethylenimines (PEI; $M_W = 600$, 1800, 10,000, 70,000 g mol^{-1}), as seen in Figure 2(a), and polypropylene acyloxy ethyl trimethylammonium chloride (PDAC), as seen in Figure 2(c), were purchased from Aladdin Co., Ltd, Shanghai, China. Pure polyvinylamine (PVAM; $M_W = 200{,}000$ g mol^{-1}), as seen in Figure 2(b), toluidine blue (TB), and poly (vinyl alcohol potassium sulfate) (PVSK) were purchased from Dia-Nitrix Co., Ltd., Tokyo, Japan. Industrial polyester film, PET (type, 6020; thickness, 160 μm) was purchased from Yuxiang Electronic Material Co. Ltd, Shanghai, China.

Substrate Pretreatment

A PET film was used as the deposition substrate for the gas barrier measurements. The film was cleaned with ultrapure water and ethanol and then pretreated with an alkali–amine solution prepared by mixing with sodium hydroxide (8.4%) and ethylenediamine (0.6%). The PET film was dipped into the alkali–amine solution at 70°C for 1 h, the film was then rinsed with ultrapure water, and dried before the LBL assembly. After pretreatment, the water contact angle of the PET surface decreased from 60° to 48° (Figure 3), indicating that the oxidation process made the surface of the membrane more hydrophilic and conducive for the adsorption of the first layer.

Layer-By-Layer Assembly

First, the pretreated substrate (PET film) was dipped into a positively charged solution (PEI, PVAM, and PDAC solution, 1 wt %) for 30 min. After rinsing with ultrapure water and drying on a spin coater, the PET film was dipped into a negatively charged solution (GO, 1 wt %) for 30 min, then rinsed and dried again. This process (Figure 4) was one deposition cycle and produces one bilayer. This entire process was repeated to prepare composites with an increasing number of bilayers. The PEI/GO film properties were controlled by adjusting various experimental conditions including the solution concentration, molecular weight of PEI, number of bilayer, drying method and dipping time. In order to isolate their effects, these parameters were varied independently of one another, with the others remaining constant as described below. (1) When the solution concentrations were changed (when the PEI concentration was changed, the GO concentration was held at 0.5 wt %; when the GO concentration was varied, PEI concentration was kept at 1 wt %.), the molecular weight of PEI is 10,000 g mol^{-1}, 10 bilayers were assembled, the soaking time was 30 min and the samples were dried by spin drying. (2) When the molecular

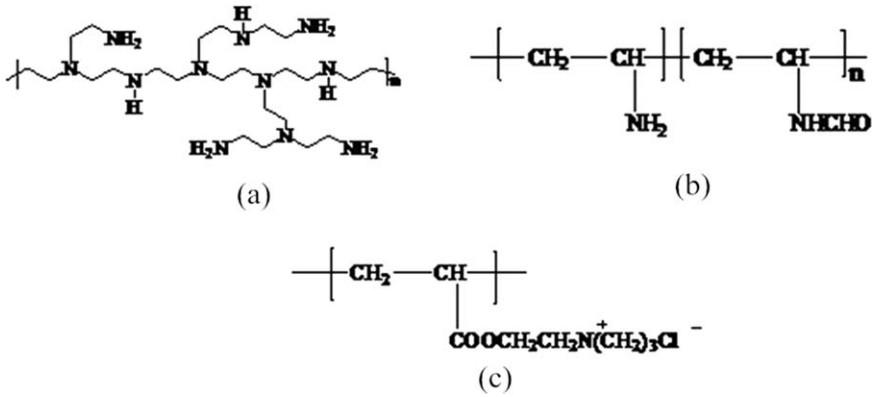

Figure 2. (a) Polyethylenimines (PEI), (b) polyvinylamine (PVAM), and (c) polypropylene acyloxy ethyl trimethylammonium chloride (PDAC).

weight of PEI was varied, the experimental conditions were kept as above and the PEI concentration was held at 1 wt % and the GO concentration was held at 0.5 wt %, which is written as $(PEI_1/GO_{0.5})$. (3) When changing the number of bilayers, the $(PEI_1/GO_{0.5})$ was assembled with 30 min of soaking time, was spin dried and had a PEI molecular weight of 10,000 g mol^{-1}. (4) When the drying method was varied, the $(PEI_1/GO_{0.5})$ was assembled with 30 min of soaking time, had a PEI molecular weight of 10,000 g mol^{-1} and 10 bilayers, which is written as $(PEI_1/GO_{0.5})_{10}$. Finally, (5) when the soaking time was varied, the $(PEI_1/GO_{0.5})_{10}$ was spin dried, and the PEI molecular weight was 10,000 g mol^{-1}.

Testing and Characterization

The film thickness on silicon wafers was measured with an alpha-SE Ellipsometer (J.A. Woollam Co. Inc., EC-400 and M-2000V) by taking the average of three measured thickness values. The absorbance of the membrane was measured by UV–Visible spectroscopy in the wavelength range of 190 to 550 nm. The composite film was cut to an appropriate size and inserted into a standard quartz cell (thickness, 1 mm). After establishing a baseline calibration using a blank sample (a film without bilayers), the UV–Visible spectra of the membranes with different layers were measured. The membrane morphologies (top layer and cross-section) were observed by scanning electron microscopy (SEM; Hitachi S-4800, Japan) with gold sputtered coated layers. In order to observe the cross-section of the membrane, the membrane was freeze-fractured using liquid nitrogen. The surface morphologies of the coated PET substrates were imaged using a multimode scanning probe microscope (AFM; Veeco Digital Instruments, Santa Barbara, CA) operated in a tapping mode. The performance of the films as hydrogen gas barriers were measured using a pressure permeation instrument (Labthink Instruments Co., Ltd.) at 23°C and 50% relative humidity (RH). A differential pressure of 0.1 MPa was maintained during the measurement to determine the gas transmission rate, permeability, solubility, and diffusivity. Charge density of different polyelectrolytes was determined by colloid titration[34] using poly(vinyl potassium sulfate) (PVSK).

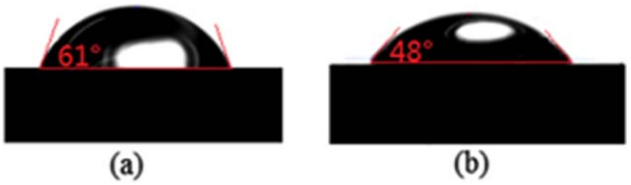

Figure 3. Water contact angle of the membrane for: (a) untreated film, and (b) treated film. [Color figure can be viewed in the online issue, which is available at wileyonlinelibrary.com.]

RESULTS AND DISCUSSION

The Performance of the Polyelectrolyte/Graphene Oxide Layer-By-Layer Assembly Films as Hydrogen Gas Barriers

In this study, PET substrates with multilayer films composed of different positively charged polyelectrolytes (branched PEI, 70000 g mol^{-1}; PVAM, 300,000 g mol^{-1}; PDAC, 1 wt %) and negatively charged materials (GO, 1 wt %) were fabricated by the LBL assembly technique. As shown in Figure 5, for the PEI/GO system, the membrane fabrication started with the adsorption of the positively charged PEI layer with a branched structure onto a pretreated negatively charged PET substrate. Then, GO sheets, functionalized with phenolic OH and COOH groups, were adsorbed onto the positively charged PEI-coated surface. The alternating sequential adsorption of PEI and GO layers resulted in the wall structure of a multilayer film on the PET substrate.

Figure 6 shows the hydrogen gas barrier performance of multilayer films composed of different positively charged polyelectrolytes and GO. Among the three systems, the PDAC/GO system exhibited the highest charge density as well as worst hydrogen gas barrier performance. This is due to the many acyloxy groups in PDAC molecule (Figure 2). This functional group is quite

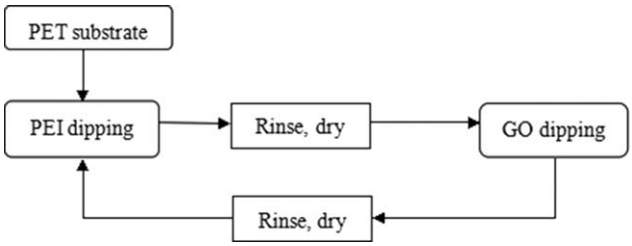

Figure 4. Layer-by-layer assembly process of PEI/GO.

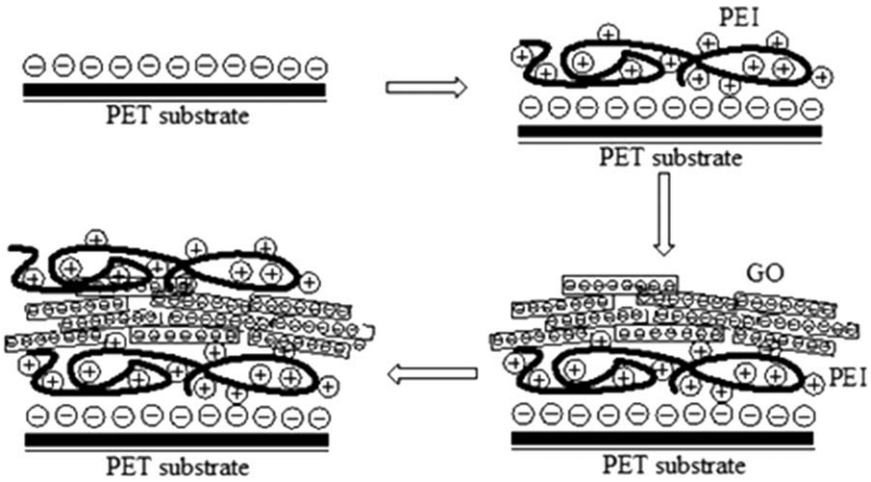

Figure 5. Mechanism of PEI/GO layer-by-layer assembly.

rigid and causes a large intramolecular gap and weaker interlayer bonding force, as has been previously reported for PDAC-polymer assembly.[35] Moreover, the chloride ion on the molecular chain has electric charge effect. Both of these factors reduce the adsorption of GO, causing the formation of a thin GO layer that is not dense enough to effectively reduce H_2 gas permeability. PVAM, with a molecular weight of 100,000 g mol^{-1}, has a long linear molecular chain and also high charge density. Because of its large electrical charge density, PVAM could easily self-assemble with GO; however, excess positive charge on the PVAM molecule also resulted in a large repulsive force between the molecular chains. Ideally, the charge density between the polyelectrolytes should be matched in order to be conducive to assembly.[36] For PVAM, the number of polymer molecular chains adsorbed on the substrate was reduced, and the gap between the adsorbed polymer molecular chains was increased. The loose PVAM film did not adsorb a sufficient quantity of GO sheets to prevent gas permeation. As seen in Figure 6, the hydrogen gas transmission rates (H_2TR) of PVAM/GO and PDAC/GO films are slightly enhanced. As shown in Figure 2(a), the branched structure of PEI molecular chain makes a planar adsorption structure on the surface of the PET film, and many secondary amine groups on the molecular chain form positively charged ions, thus facilitating the adsorption process. The planar structure of PEI is then able to smoothly adsorb the GO sheets, finally forming a wall-like structure with reduced H_2 permeability.

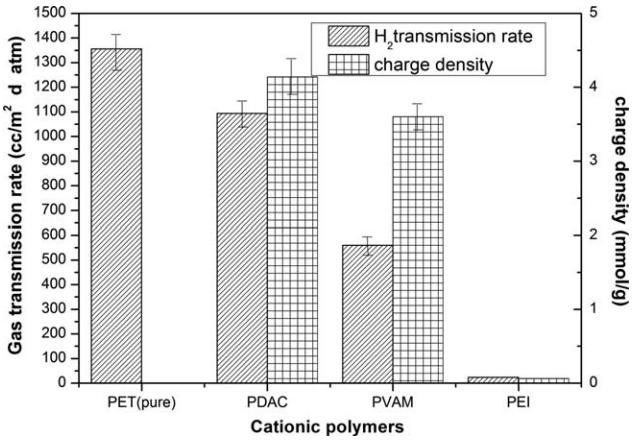

Figure 6. Hydrogen transmission rates of multilayer films composed of different positively charged polyelectrolytes and graphene oxide (every sample was measured three times to calculate the error bars).

Hydrogen Gas Barrier Performance of Multilayer Films Composed of Polyethylenimines and Graphene Oxide

The experimental results showed that multilayer films composed of PEI and GO exhibited the best hydrogen gas barrier performance. Next, the effects of the molecular weight of PEI, concentrations of PEI and GO, number of bilayers, soaking time, and drying methods on the hydrogen-resisting performance of PEI/GO multilayer membranes were investigated.

Figure 7 shows the transparency of PEI/GO composite films prepared with different molecular weights of PEI. For $(PEI/GO_1)_{10}$, most of prepared film looks uniform and transparent, which also shows the thickness of the deposited film is very thin. However, the PEI with a molecular weight of 600 g mol^{-1} could not properly assemble with GO to make a homogeneous coating. The hydrogen transmission rates of the PEI/GO films deposited on the PET substrate were tested at 23°C and 50% RH (Figure 8). The PEI/GO LBL-assembled films that were prepared from the PEIs with molecular weights of 1800 and 10,000 g mol^{-1} exhibited

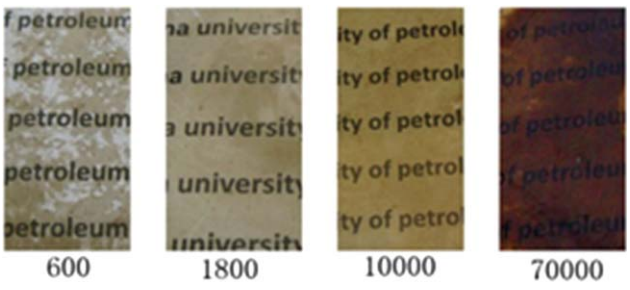

Figure 7. Transparency of PEI/GO composite films prepared from PEIs with different molecular weights. [Color figure can be viewed in the online issue, which is available at wileyonlinelibrary.com.]

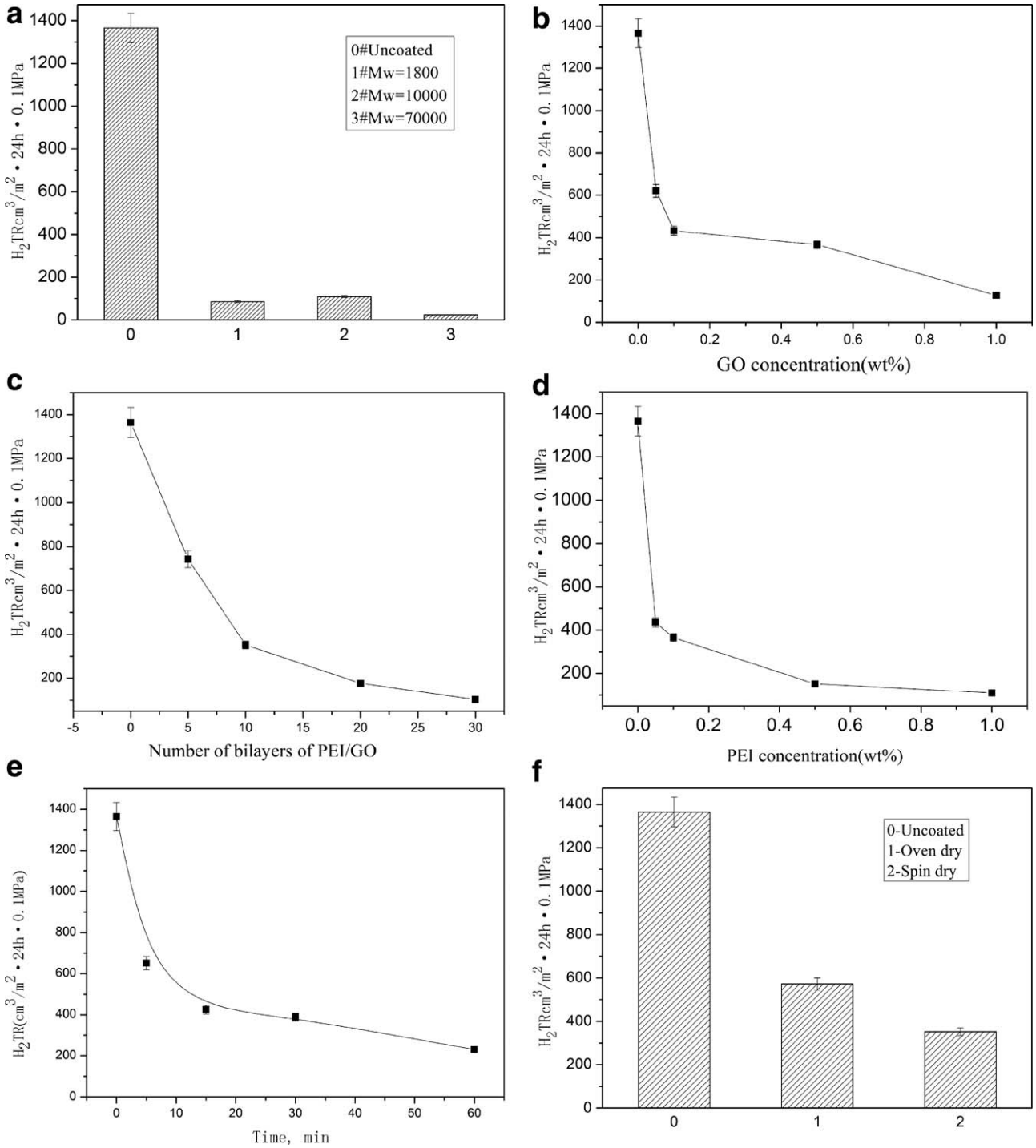

Figure 8. Hydrogen transmission rate of PEI/GO assemblies on PET measured at 23°C and 50% RH, (a) prepared from 1 wt % GO suspensions; (b) prepared from PEI, 10,000 g mol^{-1}; (c) prepared from PEI, 10,000 g mol^{-1}, and 0.5 wt % GO suspensions; (d) prepared from 0.5 wt % GO suspensions; (e) and (f) prepared from PEI, 10,000 g mol^{-1}, and 0.5 wt % GO suspensions (every sample was measured three times to calculate the error bars).

similar hydrogen gas barrier performance. The PEI/GO film prepared from PEI with a molecular weight of 70,000 g mol^{-1} exhibited an outstanding hydrogen gas barrier performance: as seen in Figure 8(a), the H_2TR of the coated PET decreased from ~1357 to 24 $cm^3/(m^2$ 24 h 0.1 MPa) This is because the long molecular chain intertwined on the surface of the film like a woven mesh,[37] which allowed it to adsorb more GO sheets. Each GO has a large surface area, and its edges overlap with those of other GO sheets. This type of structure forms a dense coating that effectively delays the gas diffusion and improves the gas barrier performance of the film.

The H_2TR of 10-bilayer LBL-assembled films with 0.05, 0.1, 0.5, and 1 wt % GO are shown in Figure 8(b). Similar to clay/polymer LBL films,[38] the increase of GO concentration in the suspension increases the amount of GO adsorbed on the PET substrate, which leads to more overlapping of the platelets and extends the diffusion pathway of the gas molecules. For $(PEI/GO_{0.5\%})$, increasing the number of bilayers from 0 to 5, 10, 20, and 30 decreased the H_2TR from 1357 to 742, 352, 177, and 103 $cm^3/m^2 \cdot 24\ h \cdot 0.1\ MPa$, respectively [Figure 8(c)]. The $(PEI/GO_{0.5\%})_{30}$ LBL-assembled film reduced the H_2TR by more than an order of magnitude relative to the uncoated PET substrate. Additionally, while holding the GO concentration constant, increasing the PEI concentration also improved the gas barrier performance of the system [Figure 8(d)]. Figure 8(e) clearly shows the adsorption equilibrium process: the H_2TR decreased non-linearly with increasing soaking time. Figure 8(f) shows the different gas barrier effects observed by using different drying methods. The results clearly show that spin drying was better; this is because the GO layers could spread on the film surface more evenly because of centrifugal force.

Characterization of Multilayer Films Composed of Polyethylenimines and Graphene Oxide

Figure 9 shows the transparency of PEI/GO multilayer films with different numbers of bilayers. The absorbance was also monitored by UV–Visible adsorption spectra; Figure 10(a) shows a series of adsorption curves of the respective layer components. The absorbance of the multilayer films at 260 nm increased linearly with the number of bilayers, as shown in Figure 10(b). Consistent with the adsorption spectra, the ellipsometric measurement showed that the thickness of multilayer films was linearly proportional to the number of bilayers.

Figure 11 shows the surface SEM images of the PEI/GO membranes with different numbers of bilayers. Before coating, the surface of the PET substrate was a little rough because of treatment by lye [Figure 11(a)]. However, after 10 bilayer coatings, the surface of the membrane became smooth and some relatively large areas of GO sheet stacking can be observed [Figure 11(b)]. The AFM micrographs (Figure 12) also show that the surface of the PET substrate film is very flat and smooth after the adsorption of three bilayers of PEI and GO. Clearly, this smoothness is donated by the smooth structures of PEI and GO completely adsorbed on the substrate film surface, covering it completely. This formed an effective gas barrier layer and as

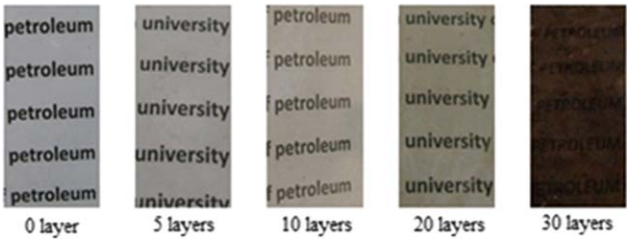

Figure 9. Transparency of PEI/GO composite films with different bilayers. [Color figure can be viewed in the online issue, which is available at wileyonlinelibrary.com.]

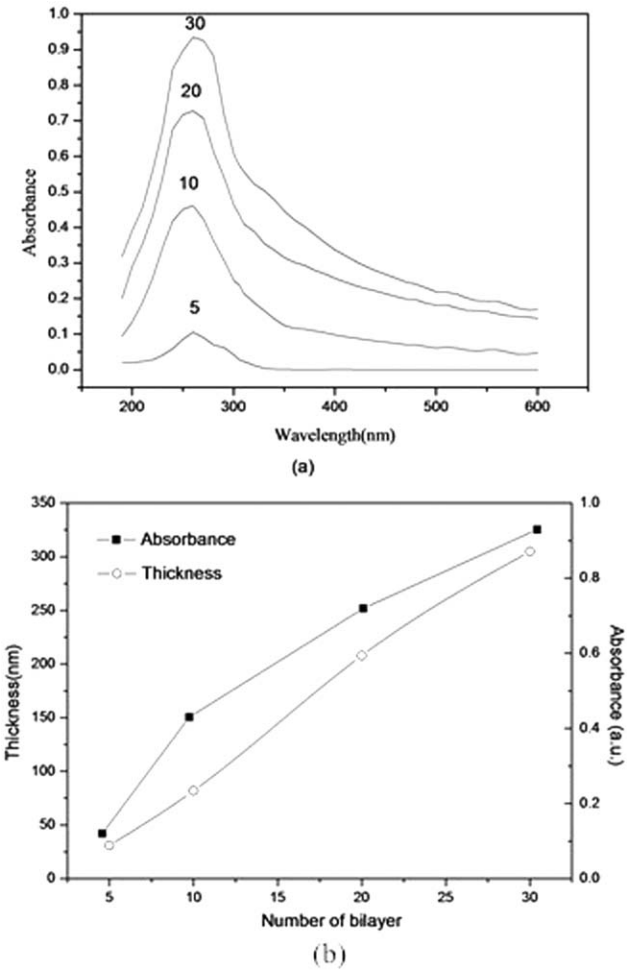

Figure 10. Growth curve of PEI/GO membranes with different bilayers. (a) UV/Vis spectra of the multilayer and (b) a plot of the thickness and absorbance with respect to the number of bilayers.

such, improved the gas barrier performance of the film. As shown in Figure 8(c), the H_2TR decreases quickly with an increasing number of bilayers. However, this decrease of H_2TR slows after more than 10 bilayers have been adsorbed, which may because the surface of the film becomes a little rough.

As shown in Figure 11(c), the PET substrate adsorbed 30 bilayers of PEI/GO LBL-assembled film. Folds are clearly observed on the surface of the membrane. Thus, during the LBL assembly, many GO sheets are adsorbed onto the branched PEI because of powerful charge interactions of PEI. The GO sheets may overlap and spread on the surface of the PEI coat. As the number of bilayers increases, the PEI/GO multilayer became thicker and several folds appear on the surface of the membrane. This roughness due to the folds on the surface causes the H_2TR to decrease with the number of bilayers more slowly [as shown in Figure 8(c)]. Therefore, the smoothness and density of the layer structure plays an important role in hindering the transmission of H_2. The SEM cross-section images (Figure 13) clearly show the loading of GO. The thickness of ultrathin

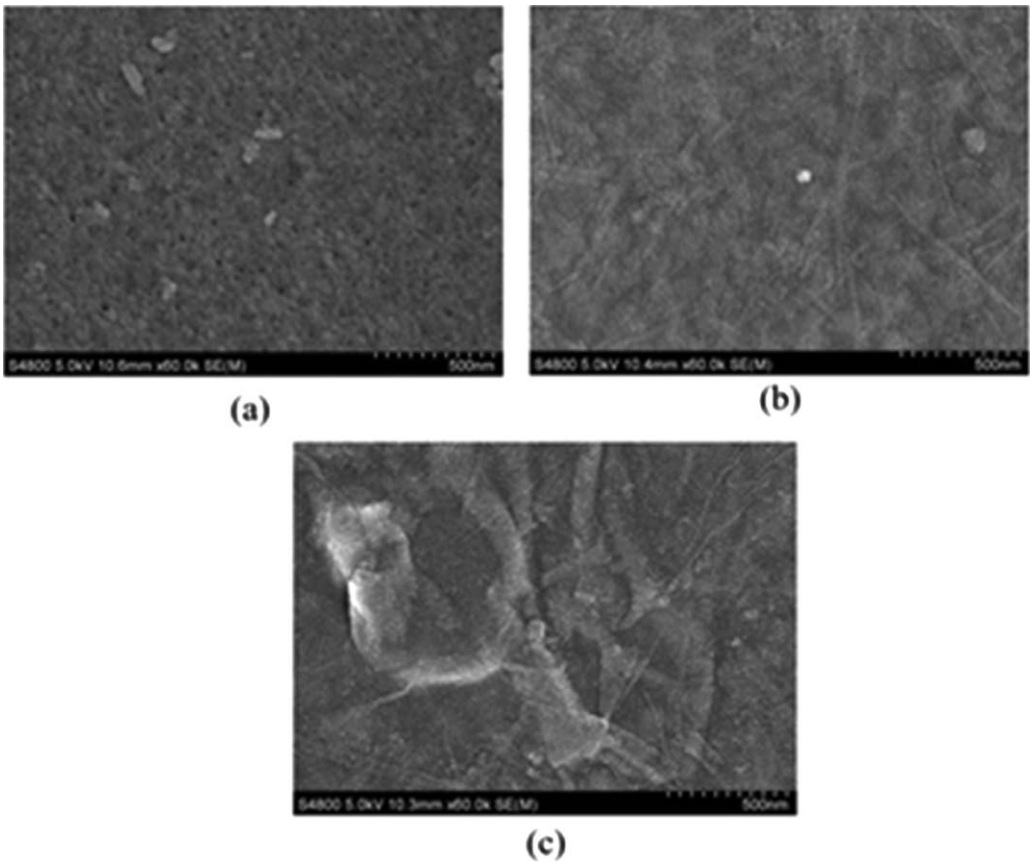

Figure 11. Surface SEM images of the PEI/GO membranes with different bilayers: (a) 0 bilayers, (b) 10 bilayers, and (c) 30 bilayers.

membrane prepared by self-assembly is on the nanoscale. Its lamellar structure forms a dense gas barrier layer, which played an important role in improving the gas barrier performance of the basement film. The thickness of $(PEI/GO)_5$ deposited films was 33 nm and the $(PEI/GO)_{10}$ was 83 nm.

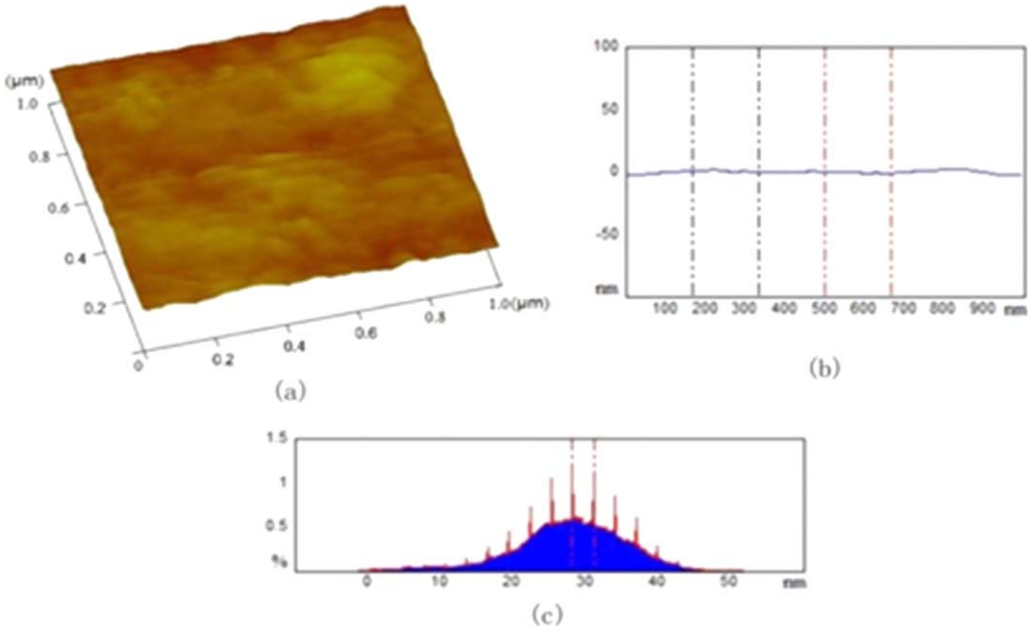

Figure 12. AFM images of PEI/GO membrane with three bilayers. [Color figure can be viewed in the online issue, which is available at wileyonlinelibrary.com.]

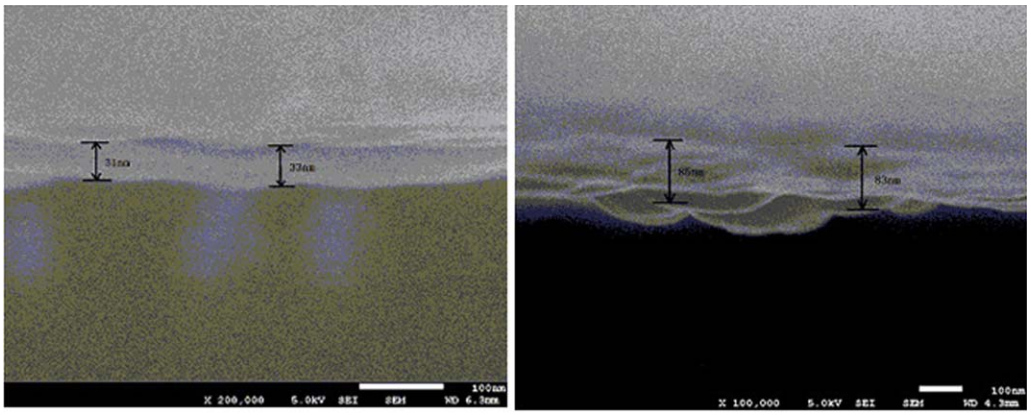

Figure 13. SEM cross-section images of PEI/GO membrane with different bilayers: (a) 5 bilayers, (b) 10 bilayers. [Color figure can be viewed in the online issue, which is available at wileyonlinelibrary.com.]

CONCLUSIONS

Different positively charged polyelectrolytes and negatively charged GO were chosen to prepare LBL-assembled composite coatings on a PET substrate. Among these ultrathin films, the multilayer film composed of PEI and GO exhibited the best hydrogen gas barrier performance. The ultrathin PEI/GO LBL-assembled 10-bilayer film adsorbed on the PET surface reduced the H_2TR of the PET substrate from 1357 to 24 $cm^3/m^2 \cdot 24$ h·0.1 MPa, thus improving the hydrogen gas barrier performance of the PET film by more than an order of magnitude. Furthermore, several factors of the LBL assembly process were studied in order to find their optimal values. It was found that smaller molecular weights of PEI inhibited the formation uniformly coated self-assembled membranes; increasing the GO concentration, PEI concentration, number of bilayers, and soaking time all enhanced the gas barrier performance of the membranes nonlinearly. Additionally, the characterization of the multilayer films showed a linear increase in the film thickness with the number of bilayer coatings. The results also showed that although the multifilm had a better planarity in the beginning, the film roughness increased later while the barrier performance did not significantly improve. Therefore, a new method needs to be developed to ensure film planarity and covering to effectively improve the gas barrier performance.

ACKNOWLEDGMENTS

This study was supported by the NSFC (National Natural Science Foundation of China) under Grant 51203186, the Converging Research Center Program funded by Korean Ministry of Education (2013K000415), the Project of Science and Technology Program for Basic Research of Qingdao (No. 12-1-4–7-(6)-jch), and the Fundamental Research Funds for the Central Universities.

REFERENCES

1. Phillips, C. A. *Int. J. Food. Sci. Tech.* **1996**, *31*, 463.
2. Bhattacharya, S. K.; Tummala, R. R. *Microelectr. J.* **2001**, *32*, 11.
3. Erlat, A. G.; Henry, B. M.; Ingram, J. J.; Mountain, D. B.; McGuigan, A.; Howson, R. P.; Grovenor, C. R. M.; Briggs, G. A. D.; Tsukahara, Y. *Thin Solid Films* **2001**, *388*, 78.
4. Creatore, M.; Palumbo, F.; Agostino, R.; Fayet, P. *Surf. Coat. Tech.* **2001**, *142*, 163.
5. Roberts, A. P.; Henry, B. M.; Sutton, A. P.; Grovenor, C. R. M.; Briggs, G. A. D.; Miyamoto, T.; Kano, A.; Tsukahara, Y.; Yanaka, M. *J. Membr. Sci.* **2002**, *208*, 75.
6. Okamoto, M.; Morita, S.; Kotaka, T. *Polymer* **2001**, *42*, 2685.
7. Ren, J. X.; Sliva, A. S.; Krishnamoorti, R. *Macromolecules* **2000**, *33*, 3739.
8. Ray, S. S.; Maiti, P.; Okamoto, M.; Ueda, K. *Macromol. Rapid. Commun.* **2002**, *23*, 943.
9. Zhang, X.; Li, S.; Jin, X.; Zhang, S. *Chem. Commun.* **2011**, *47*, 4929.
10. Hong, T. K.; Lee, D. W.; Choi, H. J.; Shin, H. S.; Kim, B. S. *ACS Nano* **2010**, *4*, 3861.
11. Pei, R.; Cui, X.; Yang, X.; Wang, E. *Biomacromolecules* **2001**, *2*, 463.
12. Kotov, N. A. *Nanostruct. Mater.* **1999**, *12*, 789.
13. Kim, B. S.; Park, S. W.; Hammond, P. T. *ACS Nano* **2008**, *2*, 386.
14. Serizawa, T.; Nanameki, K.; Yamamoto, K.; Akashi, M. *Macromolecules* **2002**, *35*, 2184.
15. Priolo, M. A.; Gamboa, D.; Holder, K. M.; Grunlan, J. C. *Nano Lett.* **2010**, *10*, 4970.
16. Yang, Y. H.; Haile, M.; Park, Y. T.; Malek, F. A.; Grunlan, J. C. *Macromolecules* **2011**, *44*, 1450.
17. Novoselov, K. S.; Geim, A. K.; Morozov, S. V.; Jiang, D.; Zhang, Y.; Dubonos, S. V.; Grigorieva, I. V.; Firsov, A. A. *Science* **2004**, *306*, 666.
18. Novoselov, K. S.; Geim, A. K.; Morozov, S. V.; Jiang, D.; Katsnelson, M. I.; Grigorieva, I. V.; Dubonos, S. V.; Firsov, A. A. *Nature* **2005**, *438*, 197.

19. Stankovich, S.; Dikin, D. A.; Dommett, G. H. B.; Kohlhaas, K.; Zimney, E. J.; Stach, E.; Piner, R.; Nguyen, S.; Ruoff, R. *Nature* **2006**, *442*, 282.

20. Balandin, A. A.; Ghosh, S.; Bao, W. Z.; Calizo, I.; Teweldebrhan, D.; Miao, F.; Lau, C. N. *Nano Lett.* **2008**, *8*, 902.

21. Zhao, X.; Zhang, Q. H.; Chen, D. J.; Lu, P. *Macromolecules* **2010**, *43*, 2357.

22. Berger, C.; Song, Z.; Li, X.; Wu, X.; Brown, N.; Naud, C.; Mayou, D.; Li, T.; Hass, J.; Marchenkov, A. N.; Conrad, E. H.; First, P. N.; de Heer, W. A. *Science* **2006**, *312*, 1191.

23. Dato, A.; Radmilovic, V.; Lee, Z.; Philips, J.; Frenklach, M. *Nano Lett.* **2008**, *8*, 2012.

24. Sutter, P. W.; Flege, J. I.; Sutter, E. A. *Nat. Mater.* **2008**, *7*, 406.

25. Fan, Z. J.; Yuan, J.; Zhi, L. J.; Zhang, Q.; Wei, T.; Feng, J.; Zhang, M. L.; Qian, W. Z.; Wei, F. *Adv. Mater.* **2010**, *22*, 3723.

26. McAllister, M. J.; Li, J. L.; Adamson, D. H.; Schniepp, H. C.; Abdala, A. A.; Liu, J.; Margarita, H. A.; Milius, D. L.; Car, R.; Prud'homme, R. K.; Aksay, I. A. *Chem. Mater.* **2007**, *19*, 4396.

27. Dreyer, D. R.; Park, S.; Bielawski, C. W.; Ruff, R. S. *Chem. Soc. Rev.* **2010**, *39*, 228.

28. Stankovich, S.; Dikin, D. A.; Piner, R. D.; Kohlhaas, K. A.; Kleinhammes, A.; Jia, Y.; Wu, Y.; Nguyen, S. T.; Ruff, R. S. *Carbon* **2007**, *45*, 1558.

29. He, H. Y.; Klinowski, J.; Forster, M.; Lerf, A. *Chem. Phy. Lett.* **1998**, *287*, 53.

30. Bunch, J. S.; Verbridge, S. S.; Alden, J. S.; van der Zande, A. M.; Parpia, J. M.; Craighead, H. G.; McEuen, P. L. *Nano Lett.* **2008**, *8*, 2458.

31. Lee, D. W.; Hong, T. K.; Kang, D. W. *J. Mater. Chem.* **2011**, *21*, 3438.

32. Yu, L.; Lim, Y. S.; Han, J. H.; Kimc, K.; Kimd, J. Y.; Choie, S.-Y.; Shin, K. *Synth. Metals* **2012**, *162*, 710.

33. Yang, Y. H.; Bolling, L.; Priolo, M. A.; Grunlan, J. C. *Adv. Mater.* **2013**, *25*, 503.

34. Kina, K.; Tamura, K.; and N. Ishibashi, *Jpn. Anal.* **1974**, *23*, 1082.

35. Tuo, X. L.; Cheng, H.; Chen, Z.; Wang, X. G. *Chem. J. Chin. Univ.* **2001**, *9*, 1581.

36. Bertrand, P.; Jonas, A.; Laschewsky, A.; Legras, R. *Macromol. Rapid Commun.* **2000**, *21*, 319.

37. Sun, B.; Jewell, C. M.; Fredin, N. J.; Lynn, D. M. *Langmuir* **2007**, *23*, 8452.

38. Jang, W. S.; Rawson, I.; Grunlan, J. C. *Thin Solid Films* **2008**, *516*, 4819.